Insights into air pollution chemistry and sulphate formation from nitrous acid (HONO) measurements during haze events in Beijing†

William J. Bloss, [iD] *[a] Louisa Kramer,‡[a] Leigh R. Crilley,§[a] Tuan Vu,¶[a] Roy M. Harrison, [iD] [a] Zongbo Shi, [iD] [a] James D. Lee, [iD] [b] Freya A. Squires, [iD] [b] Lisa K. Whalley,[c] Eloise Slater,[c] Robert Woodward-Massey,‖[c] Chunxiang Ye,‖[c] Dwayne E. Heard, [iD] [c] Shengrui Tong,[d] Siqi Hou,[d] Yele Sun, [iD] [e] Jingsha Xu,[a] Lianfang Wei[e] and Pingqing Fu [iD] [f]

Wintertime urban air pollution in many global megacities is characterised by episodic rapid increase in particulate matter concentrations associated with elevated relative humidity – so-called haze episodes, which have become characteristic of cities such as Beijing. Atmospheric chemistry within haze combines gas- and condensed-phase chemical processes, leading to the growth in secondary species such as sulphate aerosols. Here, we integrate observations of reactive gas phase species (HONO, OH, NO_x) and time-resolved aerosol composition, to explore observational constraints on the mechanisms responsible for sulphate growth during the onset of haze events. We show that HONO abundance is dominated by established fast gas-phase photochemistry, but the consideration of the additional formation potentially associated with condensed-phase oxidation of S species by aqueous NO_2 leading to NO_2^- production and hence HONO release, improves agreement between observed and calculated gas-phase HONO

[a]*School of Geography, Earth and Environmental Sciences, University of Birmingham, UK. E-mail: w.j.bloss@bham.ac.uk*

[b]*Wolfson Atmospheric Chemistry Laboratories, Department of Chemistry, University of York, UK*

[c]*School of Chemistry, University of Leeds, UK*

[d]*Institute of Chemistry, Chinese Academy of Sciences, Beijing, China*

[e]*State Key Laboratory of Atmospheric Boundary Layer Physics and Atmospheric Chemistry, Institute of Atmospheric Physics, Chinese Academy of Sciences, Beijing, China*

[f]*Institute of Surface-Earth System Science, Tianjin University, Tianjin 300072, China*

‡ Currently at Ricardo Energy & Environment, Harwell, Oxfordshire, OX11 0QR, UK.

§ Currently at the Department of Chemistry, York University, Toronto, ON, Canada.

¶ Currently at the School of Public Health, Imperial College London, UK.

‖ Currently at the College of Environmental Sciences and Engineering, Peking University, Beijing, 100871, China.

levels. This conclusion is highly dependent upon aerosol pH, ionic strength and particularly the parameterisation employed for S(IV) oxidation kinetics, for which an upper limit is derived.

Background

Atmospheric chemical processing leads to the removal of primary pollutants and determines the rate of production of secondary species, including ozone and many components of aerosol particles. Gas-phase processing is driven by a small number of key oxidants, of which the OH radical is predominant for the majority of species during daytime, including many hydrocarbons and inorganic gas-phase species such as SO_2 and NO_2. Gas- and condensed-phase oxidation chemistry are coupled across the two phases of aerosol, with a wide range of aqueous oxidants driving the particle phase oxidation of species such as SO_2, including NO_2 itself.

In many urban areas, particulate matter (PM, particularly $PM_{2.5}$) is a key regulated air pollutant, whose abundance drives substantial adverse human health impacts, in addition to affecting visibility, radiation transfer and amenity. PM is formed of a complex chemical mixture including both directly emitted (primary) and chemically produced (secondary) components; understanding the relationship between these underpins the accurate identification of direct and indirect PM sources, formulating the most effective and efficient clean air policy.

This challenge is emphasised by the air pollution climatology of Beijing and the North China Plain, where seasonal haze events characterised by episodic $PM_{2.5}$ excursions to 500 μg m^{-3} and above, impact the health and wellbeing of around 400 million people. Sulphate is known to be a major component of the fine size fraction of Beijing haze. The rate of formation of sulphate aerosol from SO_2, driven by chemical oxidation, is observed to increase as $PM_{2.5}$ levels rise, and recent studies into haze formation have found that the rate of production of sulphate aerosol is significantly accelerated in megacities such as Beijing.[1] New chemical mechanisms have been proposed, notably including the aqueous phase oxidation of SO_2 by NO_2, if aerosol pH is sufficiently high. A by-product of this mechanism is expected to be the production of gas-phase HONO.

Here, we analyse *in situ* observations collected during the UK–Chinese Air Pollution and Human Health (APHH) campaign in central Beijing during haze episodes in November–December 2016, which constrain the gas-phase production and removal of HONO, and the observed rate of formation of sulphate. We identify constraints from the *in situ* observations upon potential chemical SO_2 oxidation mechanisms contributing to haze formation.

Sulphate aerosol formation in haze

Secondary SO_4 formation is driven by a number of chemical mechanisms. Globally, the dominant process is the gas-phase reaction of SO_2 with OH radicals, leading to the formation of HSO_3 intermediates, which rapidly react with O_2 forming SO_3, which is converted to H_2SO_4 through reaction with water vapour. The recently characterized rapid reaction between SO_2 and criegee intermediates formed through alkene ozonolysis,[2] is unlikely to significantly impact boundary layer SO_2 oxidation due to the rapid removal of criegee intermediates by water

vapour and the water vapour dimer.[3,4] SO_2 may also partition to aqueous aerosol particles, where a series of equilibria partition between $SO_2 \cdot H_2O$ (at low pH), HSO_3^- (pH 2–7) or SO_3^{2-} under basic conditions. In the aqueous phase, SO_2 processing is driven by H_2O_2 (when pH is near neutral) and O_3 (of increasing importance under more acidic conditions). Transition metals (Fe, Mn) can also catalyse O_2 reactions leading to condensed phase sulphate formation. During the onset of haze events, sulphate formation rates of the order of tens of μg per m^3 per hour are observed.[1] Very recently, Wang et al.[5] reported the potential for HONO-mediated SO_2-to-SO_4 oxidation in Beijing cloud/fog, with associated N_2O formation.

However, current air quality models fail to reproduce elevated sulphate levels in winter haze. Several mechanisms for S(IV) oxidation are still under consideration to account for the underestimation of sulphate concentration between model simulations and field observations, including reactive nitrogen chemistry involving the oxidation of S(IV) by NO_2,[6–10] underestimation of the transient metals catalyzed pathway,[11,12] the possible oxidation on the surface of acid droplets by O_2,[13] or the otherwise dominant role of S(IV) + H_2O_2 pathway.[14] Although these pathways can improve the agreement between sulphate simulation and measurement, there remains a lack of independent constraints on modelling results, especially the potentially dominant role of the NO_2–S reaction. A tagging methodology with triple oxygen isotopes has been applied as a proxy to constrain the relative contributions of the individual oxidation pathways of S(IV),[12,15] with results showing that the NO_2–S reaction is highly dependent on pH and dominant under high-pH conditions, however, a very substantial uncertainty resulted from the assumed activity coefficient between the aerosol liquid phase ionic strength and parameterisation of the kinetic reaction rate.

The reaction between NO_2, partitioned into the aqueous phase, with HSO_3^- remains a potentially dominant driver of sulphate formation under haze conditions, forming SO_4^{2-} at rates of 1–7 μg m^{-3} h^{-1}:[6,8]

$$2NO_{2(aq)} + HSO_{3(aq)}^- + H_2O_{(aq)} \rightarrow 3H_{(aq)}^+ + 2NO_{2(aq)}^- + SO_{4(aq)}^{2-} \quad (1)$$
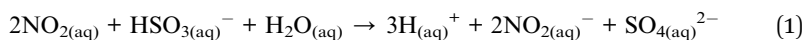
This is in contrast to tropospheric cloud processing of sulphur species, which is dominated by the H_2O_2 and O_3 reactions, with NO_2 processing relatively unimportant.[16] The mechanism has the potential to drive a positive feedback in haze formation, where increased sulphate production leads to increased aerosol water and hence SO_2 uptake and oxidation, under conditions of high NO_2.[6] Of particular note here, the condensed phase nitrite is expected to be released from acidic aerosol to the atmosphere as HONO.[8]

The ionic composition of the aqueous aerosol is critically important in calculating the importance of the NO_2 mechanism – ionic strength (which impacts the rate constants for the S(VI) oxidation reactions) and aerosol pH. Elevated pH enhances SO_2 solubility (higher effective Henry's law constant); consequently chemical factors to maintain elevated aerosol pH (5–7) are required, and have been attributed to high levels of ammonia emissions/ammonium in the North China Plain,[6,8] However, subsequent analyses have concluded that the highest observed NH_3 levels are insufficient to raise pH levels above 4.5 under haze conditions, and hence it is unlikely that NO_2-mediated oxidation of SO_2 is

a major sulphate formation route in Beijing haze, compared with O_3 and transition-metal mediated oxidation.[11]

Boundary layer HONO photochemistry

The basic gas-phase chemistry of HONO combines formation through the homogenous termolecular OH + NO reaction (R2), and reaction of HONO with OH (R3) and relatively rapid solar photolysis (R4), where the photolysis frequency (1.7×10^{-3} s^{-1} at SZA = 40°) corresponds to a typical mid-latitude local solar noon lifetime of around 10 min.

$$OH + NO + M \rightarrow HONO + M \qquad (2)$$

$$HONO + OH \rightarrow H_2O + NO_2 \qquad (3)$$

$$HONO + h\nu \rightarrow OH + NO \qquad (4)$$
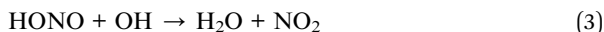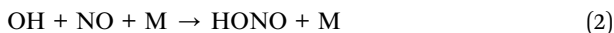
HONO photolysis (R4) is an important, and frequently the dominant, source of OH radicals in the continental boundary layer, accounting for 40% of OH formation in central London,[17] over 80% of OH production at a rural site in Colorado,[18] and most recently an average of 83% of OH production in wintertime Beijing[19] – hence, HONO abundance and formation mechanisms are tightly coupled to the production of OH and rate of *in situ* gas-phase oxidation for many atmospheric pollutants.

HONO levels may be predicted by reactions (R2)–(R4), assuming a photochemical steady state (see below), which may then be compared with observed concentrations to ascertain the presence of additional HONO sources. This exercise has been undertaken a number of times, leading to a range of additional HONO sources being identified – which are frequently significantly larger than the homogeneous OH + NO reaction. Examples include source strengths exceeding reaction (R2) by factor 13 in a European forest,[20] 30 at Hyytiälä[21] and a factor of 19 in rural China.[22] In performing such analyses, it is important to note the timescales for HONO are rather longer than those of OH, hence analysis in highly spatially heterogeneous environments can be challenging as noted by Lee *et al.*[23] and Crilley *et al.*[24]

In general terms, such sources may be combined as an additional source term, S_{HONO}, if HONO may be placed into the steady state:

$$S_{HONO} \rightarrow HONO \qquad (5)$$

$$d[HONO]/dt = k_2[OH][NO] + S_{HONO} - k_3[OH][HONO] - j_4[HONO] \qquad (E1)$$

A number of mechanisms for further atmospheric HONO emission and production have been suggested. Direct emission sources include vehicle exhausts (with HONO emissions equivalent to 1.24%, and 0.85% of NO_x emissions recently derived for the Hong Kong and UK vehicle fleets, respectively),[25,26] biocrusts,[27] and microbial soil emissions.[28] Heterogeneous HONO sources include dark reactions between NO_2 and water (*e.g.* Finlayson-Pitts *et al.*[29]) on ground and aerosol surfaces, photolysis of nitrophenols, and photoenhanced conversion of NO_2 to HONO in the presence of organic chromophores.[30]

Substantial work has been undertaken and the reader is directed to the reviews of Kleffman[31] and Spataro and Ianniello.[32]

The UK–Chinese Air Pollution and Human Health – Beijing experiment (APHH-Beijing), was funded by the UK Natural Environment Research Council and the National Science Foundation of China. APHH-Beijing brought together well over 100 instruments to study boundary layer atmospheric composition and haze formation at the Institute of Atmospheric Physics (IAP), Chinese Academy of Sciences in central Beijing in November–December 2016 and spring–summer 2017.

Here, we combine co-located measurements from the APHH study, alongside numerical model calculations, to explore potential constraints on the sulphate formation mechanisms under haze conditions in Beijing. We compare the abundance of HONO with potentially determinant parameters including PM, meteorological factors and aerosol composition (including SO_4). We calculate the HONO concentrations which would be predicted in ambient air from established gas-phase chemistry (reactions (2)–(4)), and the rate of HONO formation from the aerosol-mediated NO_2/SO_2 oxidation process (reaction (1)). We compare predicted HONO levels with those observed, and discuss the quantitative agreement in the context of different approaches to parameterising the NO_2-enhanced SO_2 oxidation kinetics. Implications for air quality are discussed.

APHH-Beijing measurements

Measurements were acquired during the APHH-Beijing winter experiment, conducted from 10 November–10 December 2016 at the Institute of Atmospheric Physics (IAP), Chinese Academy of Sciences in central Beijing $39°58'33''$ N, $116°22'41''$ E, between the third and fourth North ring roads. The site is in a residential area, with a number of substantial highways ca. 150 m away to the south, north and west. On the site itself, an open grassed area is surrounded by 2–3 storey buildings, with larger structures (residential blocks) some 200–300 m away. A canal runs past the north perimeter of the site, with a park (including conifer pine trees) further to the west. Given recent work to relocate industry from central Beijing, the dominant local emission sources are anticipated to be traffic and domestic activities, with possible contributions from light industry, for NO_x. For SO_2, sources are anticipated to be regional, industry and power/heating-related combustion (including coal) around the city periphery. For full details of the site, instruments and campaign overview, including a detailed meteorological timeseries, see Shi et al.[33]

OH radicals were measured via laser-induced fluorescence, using the fluorescence assay by gas expansion (FAGE) methodology. Full details of the instrument operation and calibration are given in Slater et al.[19] NO was measured using chemiluminescence employing a Thermo TE42i NO_x monitor, calibrated to an NPL α-standard. Photolysis frequencies (j_{HONO}) were measured at ground level using a calibrated spectral radiometer. HONO was measured using the LOPAP (Long Path Optical Absorption Photometry) approach. The LOPAP is a wet chemical technique and has been described in detail in Heland et al.[34] and Kleffmann et al.[35] Briefly, a stripping coil entrains gas-phase HONO into an acidic solution where it is derivatized into an azo dye, detected by long path absorption at 550 nm, and calibrated against an aqueous phase nitrite standard. The LOPAP

was operated and calibrated according to the standard procedures described in Kleffmann and Wiesen.[36] A detailed account of the APHH-Beijing HONO dataset, including an intercomparison of HONO measurements by LOPAP, broadband cavity absorption spectrometry, chemical ionisation mass spectrometry and proton transfer reaction mass spectrometry is given in Crilley *et al.*[37] All data were acquired at ground level (inlet heights = 5 m).

Aerosol data for sulphate mass concentration were taken from AMS (aerosol mass spectrometer) measurements; these therefore correspond to the fine fraction (PM_1) of the particulate matter present. The sulphate concentrations determined by AMS data were compared with the results obtained by 24 hour high-volume $PM_{2.5}$ filter samples collected at the IAP site during December 2016, and analysed in the laboratory by ion chromatography.[38] The two datasets were found to be within 20% of each other ($r^2 = 0.97$) and the AMS data were used without further adjustment. $PM_{2.5}$ mass concentrations were derived by TEOM-FDMS, and were recorded at the top of a two-storey building (about 10 m above ground level). Data were averaged to hourly mean mixing ratios using *in situ* temperature and pressure measurements. The period 2–10 December was selected as this encompassed several periods of haze, with rapid and dramatic $PM_{2.5}$ growth reaching nearly 500 µg m^{-3} (haze periods typically identified as $PM_{2.5}$ > 75 µg m^{-3}), and maximised overlap between the operational periods of the various instruments used – during this date range, 65% of the necessary

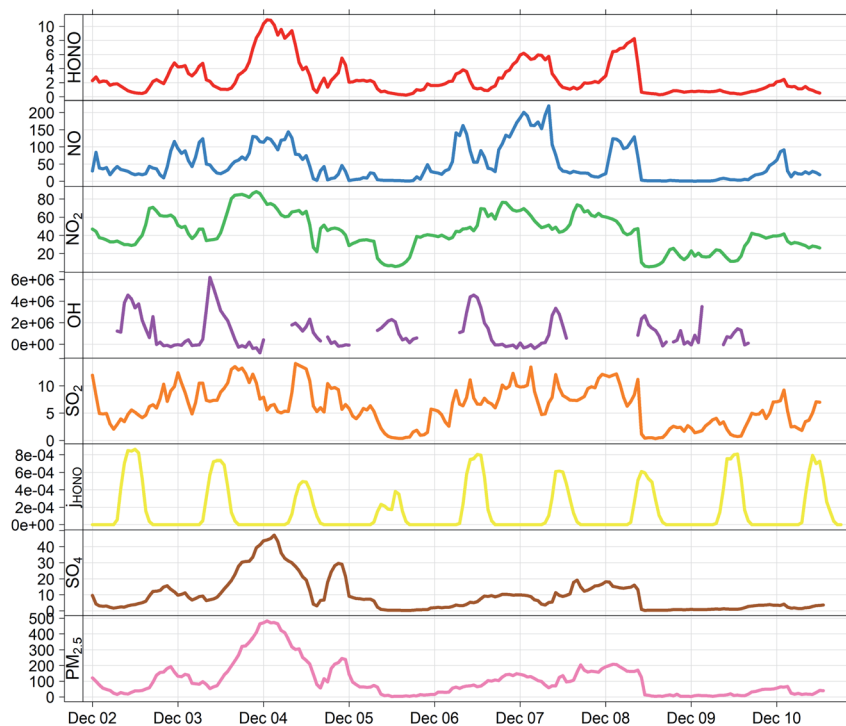**Fig. 1** Measured timeseries for HONO (ppb), NO (ppb), NO_2 (ppb), OH (molec cm^{-3}), SO_2 (ppb), j_{HONO} (s^{-1}), SO_4 (AMS; µg m^{-3}) and $PM_{2.5}$ (TEOM FDMS; µg m^{-3}) at the IAP tower site during the APHH Beijing winter campaign, 2016.

measurements were present (see Fig. 1), limited primarily by the OH and HONO datasets. Conditions during this period were typical of the wider APHH winter campaign (see Shi *et al.*[33] for climatological details).

Analysis of *in situ* observations

Fig. 1 shows the characteristic pattern of haze event onset observed previously, and associated with increases in many air pollutant species and intermediates; daily mean mixing ratios/concentrations are given in ESI Tables ST1 and ST2.† There is a positive correlation between HONO and sulphate abundance, indicating commonality in their mechanisms of formation/removal. In general, HONO abundance is frequently closely coupled with that of NO_2 (through heterogeneous NO_2-to-HONO conversion chemistry, and/or co-emission of both species), and variations in the HONO/NO_2 ratio can be used to characterise this relationship. We find HONO levels are correlated with the abundance of $PM_{2.5}$ ($r^2 = 0.67$) and of aerosol sulphate ($r^2 = 0.59$), but the HONO/NO_2 ratio is much less strongly related to $PM_{2.5}$ abundance ($r^2 = 0.27$), indicating that the interaction between particulate matter and HONO may be more strongly related to sulphate chemistry, than NO_2-to-HONO heterogeneous conversion. The HONO–SO_4 relationship does not show any dependence upon SO_2, but higher levels of both species are strongly associated with higher RH (Fig. 2), indicating a potential association with aqueous content, such as the condensed phase SO_2 oxidation mechanisms outlined above.

The measurement data coverage during the APHH-Beijing campaign at IAP provides direct constraints on the major (gas-phase, photochemical) processes forming and removing ambient nitrous acid, including measurements of concentrations of OH, NO, HONO and meteorological/photolysis parameters. We averaged data to an hourly time resolution, and evaluated the consecutive changes in concentration of HONO (*i.e.* d[HONO]/dt, defined simply as the difference in consecutive hourly mean measurements of HONO abundance), and
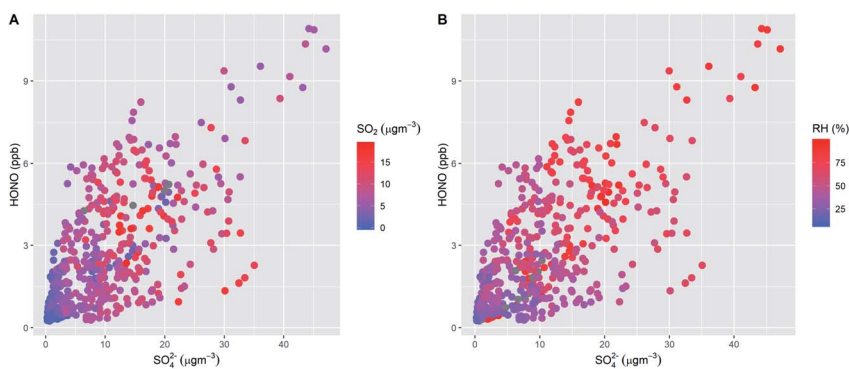
Fig. 2   Relationship between HONO and SO_4 concentrations, coloured by SO_2 abundance (panel A) and by relative humidity (RH, panel B), during the 2–10 December focus period. The data show the limited impact of SO_2, but the highest levels of both HONO and SO_4 are associated with elevated humidity.

Faraday Discussions

rate of the chemical reactions forming and removing HONO over the equivalent time periods (E1).

Fig. 3 shows the derived timeseries for d[HONO]/dt, and the individual components of HONO formation and removal, focusing upon the case study period of 2–10 December. The dominance of the conventional gas-phase chemistry is apparent, with HONO formation dominated by the OH + NO reaction, and removal by photolysis, with a small to negligible contribution from the OH + HONO reaction.

Discounting potential additional sources of HONO (*i.e.*, assuming $S_{HONO} = 0$), we can calculate the HONO abundance that would be predicted assuming the steady state applies. We limit the analysis to daylight only (here, hourly-averaged data where the HONO lifetime is less than 60 min), corresponding to $j_{HONO} > 2.78 \times 10^{-4}$ s^{-1}, and where all measurements are available (HONO, OH, NO, SO$_2$, photolysis parameters, aerosol composition) – this condition reduces the available data to 44 hourly averages, 23% of the total over the focus period (the principal reduction *vs.* the coverage noted above arises due to the restriction to daylight hours). The predicted HONO concentration is compared with that observed in Fig. 4. The PSS-calculated (red triangles) and observed (blue circles) HONO mixing ratios are in relatively good agreement, indicating limited immediate need for additional production terms. A clearer picture is obtained from the regression analysis (Fig. 5), comparing the PSS-calculated and observed HONO mixing ratios (red triangles). While the data are scattered, overall the observed and calculated mixing ratios are similar in overall magnitude, without evidence for orders-of-magnitude error. Regression analysis derives gradient and intercept values of 0.90 ± 0.38 and (0.59 ± 0.84) ppb respectively (±2σ), with an r^2 coefficient of 0.35. HONO measurements performed by multiple independent techniques during the APHH-Beijing study have been compared by Crilley et al.,[37] who showed that the LOPAP-derived HONO data had a detection limit of around 35 ppt (*i.e.* very much smaller than the scatter of the observations), and that all instruments (using different techniques) were extremely well correlated with each other ($r > 0.97$), but with variations in slope (*i.e.* absolute accuracy) of 0.61–0.88.
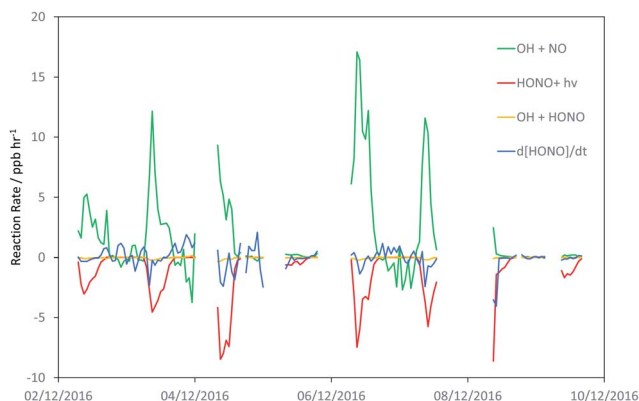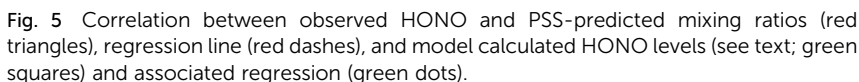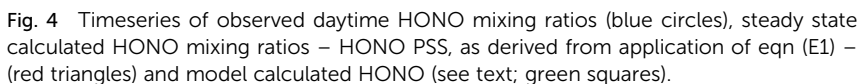

Fig. 3 Timeseries of the observationally-derived components of *in situ* HONO formation and destruction: reactions of OH + NO (R2), OH + HONO (R3), HONO + $h\nu$ (R4), plus the observed rate of change of HONO, d[HONO]/dt.

Fig. 4 Timeseries of observed daytime HONO mixing ratios (blue circles), steady state calculated HONO mixing ratios – HONO PSS, as derived from application of eqn (E1) – (red triangles) and model calculated HONO (see text; green squares).

Fig. 5 Correlation between observed HONO and PSS-predicted mixing ratios (red triangles), regression line (red dashes), and model calculated HONO levels (see text; green squares) and associated regression (green dots).

Therefore the scatter in the observed data in Fig. 4 does not reflect measurement precision (although the observations may collectively be biased high or low, depending on the absolute accuracy), and rather reflects changes in the actual observed concentrations, in turn reflecting variations in the atmospheric source and sink-terms as integrated over the HONO lifetime.

The data can also be analysed to quantify HONO formation (or removal) mechanisms not accounted for by the basic chemistry (reactions (R2)–(R4)) through application of (E1) alongside the observed $d[\text{HONO}]/dt$ to derive S_{HONO}, however the inferred net source for HONO, S_{HONO}, is very scattered and displays no correlation with SO_2 or SO_4 abundance ($r^2 = 0.04$ and 0.02 respectively), or with the SO_2-normalised rate of SO_4 formation ($r^2 = 0.05$) – not shown. A crude estimation of the rate of formation of HONO (technically, NO_2^-) which would be associated with SO_2 oxidation (P_{sulphate}) can be obtained from the observed rate of

formation of sulphate, $d[SO_4]/dt$, multiplied by a factor of 2 for the stoichiometry of NO_2^- formation:

$$P_{sulphate} = 2 \times d[SO_4]/dt \qquad (E2)$$

Critically, in addition to disregarding other (non–NO_2–mediated) mechanisms for SO_2 oxidation, this estimate for HONO formation associated with SO_4 production neglects the effect of dynamics, i.e. advection of more (or less) polluted airmasses across the study site – leading to negative as well as positive values (Fig. S1†). Nonetheless it is instructive to compare the resulting daytime $P_{sulphate}$ values, which ranged from 0.2 to 2.84 ppb h^{-1}, to those predicted for the OH + NO reaction (Fig. 3) – the $P_{sulphate}$ values are nearly one order of magnitude smaller (and likely significant overestimates during periods of haze growth, due to pollution advection).

Model quantification of SO_2 oxidation pathways

To more comprehensively quantify the relative importance of different SO_2 oxidation mechanisms and the interaction with HONO formation, a zero-dimensional numerical model constrained to the observed conditions was used to calculate the gas- and condensed-phase SO_2 oxidation rates for the focus period. The model framework involved a series of processes, consisting of gas-phase reaction of SO_2 with OH, absorption equilibria of gaseous species, ionization, aqueous phase chemical reactions of S(IV), and the kinetics of mass transport. The model assumed that air infuses into the aerosol water and then participates in chemical reactions. The condensed-phase oxidation of S(IV) by H_2O_2, O_3, oxygen catalyzed by Fe^{3+}/Mn^{2+} or NO_2 in the aerosol water were explicitly represented. The influence of primary sulphate emission and regional transportation were disregarded – the focus is on in situ chemical production only. The kinetics of sulphate formation and its dependence on ionic strength of aerosol water were implemented following Cheng et al.[6] and He et al.[15] Concentrations of Fe^{3+} and Mn^{2+} were pH-dependent and followed the precipitation equilibria of $Fe(OH)_3$ and $Mn(OH)_2$.

The Nested Air Quality Prediction Model System (NAQPMS) developed by the Institute of Atmospheric Physics, Chinese Academy of Sciences (IAP/CAS) was adopted to simulate hourly concentrations of OH free radicals and H_2O_2 during the field campaign.[39] NAQPMS incorporated the Carbon Bond Mechanism version Z (CBM-Z)[40] to simulate gas-phase reactions. The modeled OH and H_2O_2 concentrations were used in the estimation of sulphate formation from the gas-phase reaction of OH with SO_2 and the aqueous-phase reaction of H_2O_2 with HSO_3^-, and (in the case of OH) to evaluate the model oxidant field calculation. The observed aerosol composition, gaseous NH_3 and meteorological conditions were input into the ISORROPIA-II thermodynamic equilibrium model[41] to estimate the aerosol water content (AWC), aerosol water pH, and ionic strength (Table ST2†). The model was run in forward mode and predicted the phase partitioning of a $K^+/Ca^{2+}/Mg^{2+}/NH_4^+/Na^+/SO_4^{2-}/NO_3^-/Cl^-/H_2O$ in thermodynamic equilibrium with gas-phase precursors.

By way of validation, the modelled and observed OH levels[19] as a sensitive test of the integrated NAQPMS oxidation (VOC, NO_x and O_3 chemistry), are compared

in Fig. S2.† Overall, agreement was good, with the model showing good skill in reproducing the diurnal behaviour of OH. The absolute modelled OH levels were within 15% of those observed on 4 of the 6 days considered, but exceeded those observed (by up to a factor of 2) on the remaining 2 days (interestingly, those characterised by the lowest NO levels).

The modelled rate of formation of SO_4 was determined for OH (gas phase), H_2O_2, O_3, transition metals (Fe, Mn catalysed O_2 reaction) and NO_2 driven processes. Ionic strength is a key factor in such calculations: sulphate production rates were calculated for three cases: (A) neglecting the impact of ionic strength; (B) considering the impact of ionic strength upon the solubility of SO_2 and the dissociation of H_2SO_3 (ref. 42) and upon the kinetics of the H_2O_2, O_3 and transition metal reactions; and (C) also considering the impact of ionic strength upon the rate constant for the $NO_2 + S(IV)$ reaction, following the parameterisations of Cheng et al.[6] We compared these approaches as there is a lack of experimental data for the influence of ionic strength upon the NO_2–S reaction, and the calculated aerosol ionic strength during severe haze events reaches 60 M (when RH > 40% and $PM_{2.5}$ > 75 µg m^{-3}) hence extrapolations from the conditions of dilute solutions may not be warranted.

Discounting ionic strength effects (i.e., case A), SO_4 formation averaged over the whole 12 November–10 December 2016 campaign period is found to be dominated by gas-phase OH chemistry (51%), followed by condensed phase H_2O_2 and transition metal reactions, with NO_2 reaction responsible for 1.6%. Considering ionic strength effects other than NO_2 kinetics (case B), oxidation of SO_2 (g) by OH drives 81% of SO_4 formation, with 18% arising from H_2O_2 and 0.6% for reaction with NO_2 – however the average and maximum rates of SO_4 formation calculated were 0.036 and 0.29 µg m^{-3} h^{-1} respectively, much lower than those observed. Inclusion of the ionic strength parameterisation for the $NO_2 + S$ kinetics (case C) increases the calculated rate of SO_4 formation by two orders of magnitude (a factor of 96), with the calculated contribution of the NO_2 pathway for SO_4
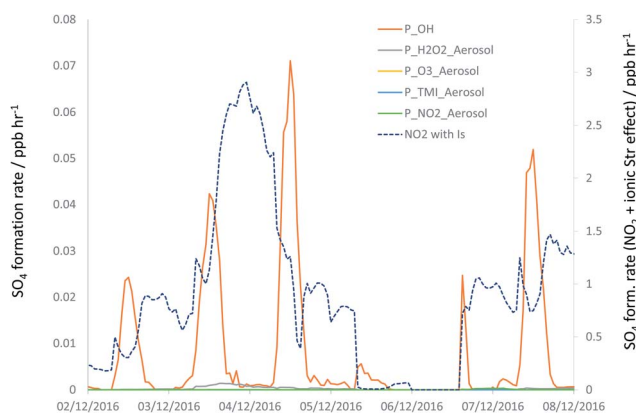

Fig. 6 Modelled SO_4 formation rates (converted to ppb h^{-1}) through reaction of SO_2 with OH (orange line), condensed phase reactions (all case B) with H_2O_2 (grey), O_3 (yellow), transition metals (blue) and NO_2 (green). Dashed line, second y axis: NO_2 reaction considering impacts of ionic strength on $NO_2 + S(IV)$ reaction kinetics (i.e. case C). See Fig. S5 (ESI†) for expansion of the H_2O_2, O_3 and TMI timeseries.

formation increasing to 98% overall, as a consequence of the very strong dependence or the rate constant upon ionic strength, highlighting this critical uncertainty in this aspect of the kinetics parameterisation. The average and maximum rates of SO_4 formation calculated for case C were 3.5 and 12 µg m^{-3} h^{-1}, respectively, comparable to the behaviour observed (Fig. 1 and S3†).

The timeseries for the modelled SO_4 formation rates for each chemical mechanism under case (B), and for the NO_2-driven processing under case (C), are shown in Fig. 6 for the 2–7 December focus period – note the different y axis scale used for the latter data series (see also Fig. S4†). The significant increase in the overall rate of formation of SO_4 for case (C) is in much closer accord with the rates of SO_4 formation derived from the observed timeseries (Fig. 1), than for cases (A) and (B).

Considering the rate of production of NO_2^-, as an estimate to the HONO formation rate associated with NO_2/SO_2 oxidation, it is clear that the non-ionic-strength enhanced kinetics (case (A) and (B) – the latter as show in Fig. 6) are too small to make any appreciable impact upon HONO production, compared with the dominant OH + NO reaction flux. Calculated HONO formation from case (C), dominated by the ionic-strength-dependent reaction with NO_2, was added to the homogeneous OH + NO production to determine the impact upon calculated steady state HONO concentrations, according to eqn (E3), and as shown in Fig. 4 and 5 as HONO (+Model).

$$[HONO] = \{k_1[OH][NO] + [\text{Modelled } SO_2 + NO_2 \text{ rate}]\}/\{k_2[OH][HONO] + j_3[HONO]\} \tag{E3}$$

Addition of the $SO_2 + NO_2$ derived HONO flux increases the HONO levels by 27% on average, and modestly improves agreement between the calculated and observed HONO levels ($r^2 = 0.98$). The observed and PSS-calculated HONO levels are compared as a function of SO_4 in Fig. S3† – while higher levels of both are associated with more polluted conditions (more $PM_{2.5}$, more SO_4), no bias between the observed and PSS-calculated levels with respect to SO_4 is apparent, indicating this factor is not dominant. By applying a scale factor to the model-derived HONO production component, it can be shown that the rate of SO_2 oxidation by NO_2, as simulated here, is consistent with the observed HONO within the scatter of the data, but would cease to be so if the ionic strength enhancement factor were to be significantly increased – an upper limit (corresponding to a regression gradient of 1.5) of a factor of 4.5 fold higher may be estimated.

Conclusions

Nitrous acid was measured in the urban atmosphere of Beijing, at mixing ratios of up to 10 ppb (significantly higher than many other cities, *e.g.* 1.6 ppb for London[17]). HONO abundance, alongside that of many air pollutant species, was correlated with the formation of episodic haze events, associated with rapid growth in $PM_{2.5}$ under elevated RH conditions, including increases in sulphate concentration. The HONO abundance was correlated with that of SO_4, and with RH. The HONO/NO_2 ratio, a marker for heterogeneous interconversion of reactive nitrogen oxides to HONO through dark- and photo-enhanced reaction processes,

was not correlated with aerosol abundance, indicating heterogeneous formation does not dominate HONO production. Rather, during daytime, fast conventional gas-phase chemistry – the OH + NO reaction (2), and HONO photolysis (4) – dominates the HONO abundance in wintertime Beijing, and considering these processes (and the minor HONO + OH reaction (R3)), permits alone good quantitative agreement (regression coefficient = 0.90 ± 0.38) between measured and calculated photostationary steady state HONO levels.

Combination of observationally-constrained rates of HONO formation and loss through reactions (2)–(4), with the calculated rates of HONO production through heterogeneous mechanisms including H_2O_2, O_3, transition metal and S–NO_2 chemistry showed that, discounting the effects of ionic strength, the condensed phase mechanisms made a negligible contribution to HONO formation, while SO_2 oxidation was dominated by gas-phase OH chemistry, with the S–NO_2 reaction contributing 1.6% of the total. Inclusion of the ionic strength effects, including parameterisation of the NO_2–S(IV) kinetics following Cheng et al.,[6] led to calculated condensed-phase nitrite production equivalent to increases in the steady state HONO levels of 27%, modestly increasing agreement with the HONO levels observed. Under this scenario, the NO_2–S processing dominates SO_4 formation. Considering the constraint the HONO levels place upon the additional production attributable to the NO_2–S reaction, an upper limit to the maximum possible enhancement of the ionic-strength-dependent kinetics of a factor of 4.5 is estimated.

This work demonstrates the potential, and limitations, for coordinated observations of gaseous and particulate atmospheric composition to constrain fundamental processes which are extremely challenging to evaluate accurately in the laboratory or field – in this case, aerosol liquid water pH and ionic strength kinetic behaviour under very strongly non-ideal conditions. A key limitation of the data which are available here is their fixed measurement location: a lagrangian approach, allowing parameters to be evaluated along the trajectory of an evolving airmass at higher altitude and remote from possible surface influence may facilitate greater insight.

Conflicts of interest

There are no conflicts of interest.

Acknowledgements

References

1 B. Zheng, Q. Zhang, Y. Zhang, K. He, K. Wang, G. Zheng, F. Duan, Y. Ma and T. Kimoto, *Atmos. Chem. Phys.*, 2015, **15**, 2031–2049.

2 O. Welz, J. D. Savee, D. L. Osborn, S. S. Vasu, C. J. Percival, D. E. Shallcross and C. A. Taatjes, *Science*, 2012, **335**, 204.

3 T. Berndt, T. Jokinen, M. Sipilä, R. L. Mauldin III, H. Herrmann, F. Stratmann, H. Junninen and M. Kulmala, *Atmos. Environ.*, 2014, **89**, 603.

4 M. J. Newland, A. R. Rickard, L. Vereecken, A. Munoz, M. Rodenas and W. J. Bloss, *Atmos. Chem. Phys.*, 2015, **15**, 9521.

5 J. Wang, J. Li, J. Ye, J. Zhao, Y. Wu, J. Hu, D. Liu, D. Nie, F. Shen, X. Huang, D. D. Huang, D. Ji, X. Sun, W. Xu, J. Guo, S. Song, Y. Qin, P. Liu, J. R. Turner, H. C. Lee, S. Hwang, H. Liao, S. T. Martin, Q. Zhang, M. Chen, Y. Sun, X. Ge and D. J. Jacob, *Nat. Commun.*, 2020, **11**, 2844.

6 Y. Cheng, G. Zheng, C. Wei, Q. Mu, B. Zheng, Z. Wang, M. Gao, Q. Zhang, K. He, G. Carmichael, U. Poschl and H. Su, *Sci. Adv.*, 2016, **2**, e1601530.

7 M. Gao, G. R. Carmichael, Y. Wang, D. Ji, Z. Liu and Z. Wang, *Front. Environ. Sci. Eng.*, 2016, **10**, 16.

8 G. Wang, R. Zhang, M. E. Gomez, L. Yang, M. L. Zamora, M. Hu, Y. Lin, J. Peng, S. Guo and J. Meng, *Proc. Natl. Acad. Sci. U. S. A.*, 2016, **113**, 13630.

9 Y. Xie, A. Ding, W. Nie, H. Mao, X. Qi, X. Huang, Z. Xu, V. M. Kerminen, T. Petäjä, X. Chi, A. Virkkula, M. Boy, L. Xue, J. Guo, J. Sun, X. Yang, M. Kulmala and C. Fu, *J. Geophys. Res.*, 2015, **120**, 12679–12694.

10 R. Zhang, G. Wang, S. Guo, M. L. Zamora, Q. Ying, Y. Lin, W. Wany, M. Hu and Y. Wang, *Chem. Rev.*, 2015, **115**, 3803.

11 H. Guo, R. J. Weber and A. Nenes, *Sci. Rep.*, 2017, **7**, 12109.

12 J. Shao, Q. Chen, Y. Wang, X. Lu, P. He, Y. Sun, V. Shah, R. V. Martin, S. Philip, S. Song, Y. Zhao, Z. Xie, L. Zhang and B. Alexander, *Atmos. Chem. Phys.*, 2019, **19**, 6107–6123.

13 H.-M. Hung and M. R. Hoffmann, *Environ. Sci. Technol.*, 2015, **49**, 13768.

14 C. Ye, P. Liu, Z. Ma, C. Xue, C. Zhang, Y. Zhang, J. Liu, C. Liu, X. Sun and Y. Mu, *Environ. Sci. Technol. Lett.*, 2018, **5**, 757–763.

15 P. He, B. Alexander, L. Geng, X. Chi, S. Fan, H. Zhan, H. Kang, G. Zheng, Y. Cheng, H. Su, C. Liu and Z. Xie, *Atmos. Chem. Phys.*, 2018, **8**, 5515.

16 J. H. Seinfeld and S. N. Pandis, *Atmospheric Chemistry and Physics: From Air Pollution to Climate Change*, John Wiley & Sons, Inc., Hoboken, New Jersey, 3rd edn, 2016.

17 J. D. Lee, L. K. Whalley, D. E. Heard, D. Stone, R. E. Dunmore, J. F. Hamilton, D. E. Young, J. D. Allan, S. Laufs and J. Kleffmann, *Atmos. Chem. Phys.*, 2016, **16**, 2747.

18 S. Kim, T. C. VandenBoer, C. J. Young, T. P. Riedel, J. A. Thornton, B. Swarthout, B. Sive, B. Lerner, J. B. Gilman, C. Warneke, J. M. Roberts, A. Guenther, N. L. Wagner, W. P. Dubé, E. Williams and S. S. Brown, *J. Geophys. Res.*, 2014, **119**, 6886–6896.

19 E. J. Slater, L. K. Whalley, R. Woodward-Massey, C. Ye, J. D Lee, F. Squires, J. R. Hopkins, R. E. Dunmore, M. Shaw, J. F. Hamilton, A. C. Lewis, L. R. Crilley, L. Kramer, W. Bloss, T. Vu, Y. Sun, W. Xu, S. Yue, L. Ren,

W. J. F. Acton, C. N. Hewitt, X. Wang, P. Fu and D. E. Heard, *Atmos. Chem. Phys. Discuss.*, 2020, DOI: 10.5194/acp-2020-362.

20 J. Kleffman, T. Gavriloaiei, A. Hofzumahaus, F. Holland, R. Koppmann, L. Rupp, E. Schosser, M. Siese and A. Wahner, *Geophys. Res. Lett.*, 2005, **32**, L05818.

21 R. Oswald, M. Ermel, K. Hens, A. Novelli, H. G. Ouwersloot, P. Paasonen, T. Petäjä, M. Sipilä, P. Keronen, J. Bäck, R. Königstedt, Z. Hosaynali Beygi, H. Fischer, B. Bohn, D. Kubistin, H. Harder, M. Martinez, J. Williams, T. Hoffmann, I. Trebs and M. Sörgel, *Atmos. Chem. Phys.*, 2015, **15**, 799.

22 X. Li, T. Brauers, R. Häseler, B. Bohn, H. Fuchs, A. Hofzumahaus, F. Holland, S. Lou, K. D. Lu, F. Rohrer, M. Hu, L. M. Zeng, Y. H. Zhang, R. M. Garland, H. Su, A. Nowak, A. Wiedensohler, N. Takegawa, M. Shao and A. Wahner, *Atmos. Chem. Phys.*, 2012, **12**, 1497.

23 B. H. Lee, E. C. Wood, S. C. Herndon, B. L. Lefer, W. T. Luke, W. H. Brune, D. D. Nelson, M. S. Zahniser and J. W. Munger, *J. Geophys. Res.*, 2013, **118**, 12274–12281.

24 L. R. Crilley, L. Kramer, F. D. Pope, L. K. Whalley, D. R. Dryer, D. E. Heard, J. D. Lee, C. Reed and W. J. Bloss, *Faraday Discuss.*, 2016, **189**, 191.

25 Y. Liang, Q. Zha, W. Wang, L. Cui, K. H. Lui, K. F. Ho, Z. Wang, S. C. Lee and T. Wang, *J. Air Waste Manage. Assoc.*, 2017, **67**, 797.

26 L. J. Kramer, L. R. Crilley, T. J. Adams, S. M. Ball, F. D. Pope and W. J. Bloss, *Atmos. Chem. Phys.*, 2020, **20**, 5231.

27 B. Weber, D. Wu, A. Tamm, N. Ruckteschler, E. Rodríguez-Caballero, J. Steinkamp, H. Meusel, W. Elbert, T. Behrendt, M. Sörgel, Y. Cheng, P. J. Crutzen, H. Su and U. Pöschl, *Proc. Natl. Acad. Sci. U. S. A.*, 2015, **15**, 15384.

28 H. Su, Y. Cheng, R. Oswald, T. Behrendt, I. Trebs, F. X. Meixner, M. O. Andreae, P. Cheng, Y. Zhang and U. Pöschl, *Science*, 2011, **333**, 1616.

29 B. J. Finlayson-Pitts, L. M. Wingen, A. L. Sumner, D. Syomin and K. A. Ramazan, *Phys. Chem. Chem. Phys.*, 2003, **5**, 223.

30 C. George, R. S. Strekowski, J. Kleffmann, K. Stemmler and M. Ammann, *Faraday Discuss.*, 2005, **130**, 195.

31 J. Kleffmann, *ChemPhysChem*, 2007, **8**, 1137.

32 F. Spataro and A. Ianniello, *J. Air Waste Manage. Assoc.*, 2014, **64**, 1232.

33 Z. Shi, T. Vu, S. Kotthaus, R. M. Harrison, S. Grimmond, S. Yue, T. Zhu, J. Lee, Y. Han, M. Demuzere, R. E. Dunmore, L. Ren, D. Liu, Y. Wang, O. Wild, J. Allan, W. J. Acton, J. Barlow, B. Barratt, D. Beddows, W. J. Bloss, G. Calzolai, D. Carruthers, D. C. Carslaw, Q. Chan, L. Chatzidiakou, Y. Chen, L. Crilley, H. Coe, T. Dai, R. Doherty, F. Duan, P. Fu, B. Ge, M. Ge, D. Guan, J. F. Hamilton, K. He, M. Heal, D. Heard, C. N. Hewitt, M. Hollaway, M. Hu, D. Ji, X. Jiang, R. Jones, M. Kalberer, F. J. Kelly, L. Kramer, B. Langford, C. Lin, A. C. Lewis, J. Li, W. Li, H. Liu, J. Liu, M. Loh, K. Lu, F. Lucarelli, G. Mann, G. McFiggans, M. R. Miller, G. Mills, P. Monks, E. Nemitz, B. Ouyang, P. I. Palmer, C. Percival, O. Popoola, C. Reeves, A. R. Rickard, L. Shao, G. Shi, D. Spracklen, D. Stevenson, Y. Sun, Z. Sun, S. Tao, S. Tong, Q. Wang, W. Wang, X. Wang, X. Wang, Z. Wang, L. Wei, L. Whalley, X. Wu, Z. Wu, P. Xie, F. Yang, Q. Zhang, Y. Zhang, Y. Zhang and M. Zheng, *Atmos. Chem. Phys.*, 2019, **19**, 7519.

34 J. Heland, J. Kleffmann, R. Kurtenbach and P. Wiesen, *Environ. Sci. Technol.*, 2001, **35**, 3207.

35 J. Kleffmann, J. Heland, R. Kurtenbach, J. C. Lorzer and P. Wiesen, *Environ. Sci. Pollut. Res.*, 2002, **9**, 48.

36 J. Kleffmann and P. Wiesen, *Atmos. Chem. Phys.*, 2005, **5**, 77.

37 L. R. Crilley, L. J. Kramer, B. Ouyang, J. Duan, W. Zhang, S. Tong, M. Ge, K. Tang, M. Qin, P. Xie, M. D. Shaw, A. C. Lewis, A. Mehra, T. J. Bannan, S. D. Worrall, M. Priestley, A. Bacak, H. Coe, J. Allan, C. J. Percival, O. A. M. Popoola, R. L. Jones and W. J. Bloss, *Atmos. Meas. Tech.*, 2019, **12**, 6449.

38 J. Xu, S. Song, R. M. Harrison, C. Song, L. Wei, Q. Zhang, Y. Sun, L. Lei, C. Zhang, X. Yao, D. Chen, W. Li, M. Wu, H. Tian, L. Luo, S. Tong, W. Li, J. Wang, G. Shi, Y. Huangfu, Y. Tian, B. Ge, S. Su, C. Peng, Y. Chen, F. Yang, A. Mihajlidi-Zelić, D. Đorđević, S. J. Swift, I. Andrews, J. F. Hamilton, Y. Sun, A. Kramawijaya, J. Han, S. Saksakulkrai, C. Baldo, S. Hou, F. Zheng, K. R. Daellenbach, C. Yan, Y. Liu, M. Kulmala, P. Fu and Z. Shi, *Atmos. Meas. Tech.*, 2020, DOI: 10.5194/amt-2020-156.

39 H. Du, J. Li, X. Chen, Z. Wang, Y. Sun, P. Fu, J. Li, J. Gau and Y. Wei, *Atmos. Chem. Phys.*, 2019, **19**, 9351.

40 R. A. Zaveri and L. K. Peters, *J. Geophys. Res.: Atmos.*, 1999, **D23**, 30387.

41 C. Fountoukis and A. Nenes, *Atmos. Chem. Phys.*, 2007, 7, 4639.

42 F. J. Millero, *Mar. Chem.*, 1989, **28**, 1.